METABOLISM

Identification of entacapone as a chemical inhibitor of FTO mediating metabolic regulation through FOXO1

Shiming Peng[1]*, Wen Xiao[2]*, Dapeng Ju[1]*, Baofa Sun[2,3,4]*, Nannan Hou[1], Qianlan Liu[2,3], Yanli Wang[1], Haijiao Zhao[1], Chunchun Gao[2,3], Song Zhang[5], Ran Cao[1], Pengfei Li[1], Huanwei Huang[1], Yongfen Ma[1], Yankai Wang[1], Weiyi Lai[6], Zhixiong Ma[1], Wei Zhang[1], Song Huang[1], Hailin Wang[6], Zhiyuan Zhang[1], Liping Zhao[1], Tao Cai[1], Yong-Liang Zhao[2,3], Fengchao Wang[1], Yongzhan Nie[5], Gang Zhi[1], Yun-Gui Yang[2,3,4†], Eric Erquan Zhang[1,7†], Niu Huang[1,7†]

Recent studies have established the involvement of the fat mass and obesity-associated gene (*FTO*) in metabolic disorders such as obesity and diabetes. However, the precise molecular mechanism by which FTO regulates metabolism remains unknown. Here, we used a structure-based virtual screening of U.S. Food and Drug Administration–approved drugs to identify entacapone as a potential FTO inhibitor. Using structural and biochemical studies, we showed that entacapone directly bound to FTO and inhibited FTO activity in vitro. Furthermore, entacapone administration reduced body weight and lowered fasting blood glucose concentrations in diet-induced obese mice. We identified the transcription factor forkhead box protein O1 (*FOXO1*) mRNA as a direct substrate of FTO, and demonstrated that entacapone elicited its effects on gluconeogenesis in the liver and thermogenesis in adipose tissues in mice by acting on an *FTO-FOXO1* regulatory axis.

INTRODUCTION

Obesity and diabetes, characterized by impaired energy homeostasis and disordered body metabolism, have become severe epidemics in modern society. Genome-wide association studies have identified the fat mass and obesity-associated gene (*FTO*) as a genetic factor related to obesity (*1*–*5*). A recent study suggested that "long-range functional connections" between *FTO* intronic single-nucleotide polymorphisms and the iroquois homeobox protein 3 (*IRX3*) may promote obesity (*6*, *7*). There is also a substantial amount of evidence that FTO itself may regulate metabolic disorders (*8*–*12*). Studies in mouse models have shown that *Fto* overexpression leads to obesity, and its knockout or loss-of-function mutation results in reduced body weight (*8*–*10*). *FTO* expression in the brain has been implicated in the regulation of food intake (*13*). In adipocytes, *FTO* deficiency was reported to induce the expression of uncoupling protein 1 (*UCP1*), a mitochondrial inner membrane proton channel linked to thermogenesis (*12*). In the liver, correlations have been reported between *Fto* mRNA expression and glucose metabolism (*14*, *15*).

The FTO protein belongs to the Fe^{2+} and α-ketoglutarate (α-KG)–dependent oxygenase family (*16*, *17*). It demethylates N^6-adenosine–modified (m^6A) sites and N^6,2′-*O*-dimethyladenosine–modified (m^6A_m) sites of mRNA (*18*, *19*), thereby influencing multiple mRNA-related processes including transcript stability, alternative splicing, mRNA translocation, and protein translation (*20*–*25*). Although efforts have been made to determine the physiological and pathological relevance of FTO, how FTO is involved in metabolic regulation remains unknown, mainly due to lack of information about its definitive mRNA substrates. Furthermore, although FTO is widely viewed as an attractive biological target, it is not yet clear whether a small-molecule inhibitor specifically targeting FTO could be developed for the treatment of metabolic disorders such as obesity and diabetes. Unfortunately, only a few FTO biochemical inhibitors have been reported to date (*26*–*31*), and none have been critically evaluated for in vivo efficacy for the treatment of metabolic disorders. Thus, it is desirable to identify drug-like FTO inhibitors that may be useful in deciphering both the physiological function and potential clinical value of the FTO protein.

To uncover potential FTO inhibitors, we used a structure-based hierarchical virtual screening approach and comprehensively validated candidates using structural and biochemical experiments, in vivo experiments, and extensive transcriptome sequencing analyses. We identified entacapone, an inhibitor of catechol-*O*-methyltransferase (COMT) (*32*) used to treat Parkinson's disease, as a potent FTO chemical inhibitor. Mechanistically, FTO demethylated m^6A sites on forkhead box protein O1 (*FOXO1*) mRNA to up-regulate FOXO1 expression, thereby modulating gluconeogenesis and thermogenesis. Our studies support the potential repurposing of the U.S. Food and Drug Administration (FDA)–approved drug entacapone for the treatment of metabolic disorders such as obesity and diabetes.

RESULTS

Virtual screening and hit validation

To identify potential FTO inhibitors from FDA-approved drugs, we used a structure-based hierarchical virtual screening approach that we developed in previous studies (Fig. 1A) (*33*–*37*). We found that entacapone inhibited FTO demethylation activity at a median inhibitory concentration (IC_{50}) of 3.5 μM (Fig. 1B). Entacapone competed with both m^6A-containing oligonucleotide substrates and the

[1]National Institute of Biological Sciences, Beijing, No. 7 Science Park Road, Zhongguancun Life Science Park, Beijing 102206, China. [2]Key Laboratory of Genomic and Precision Medicine, Beijing Institute of Genomics, Chinese Academy of Sciences, No. 1 Beichen West Road, Chaoyang District, Beijing 100101, China. [3]University of Chinese Academy of Sciences, Beijing 100049, China. [4]Institute for Stem Cell and Regeneration, Chinese Academy of Sciences, Beijing 100101, China. [5]State Key Laboratory of Cancer Biology and Xijing Hospital of Digestive Diseases, Fourth Military Medical University, 127 West Changle Road, Xi'an, Shaanxi 710032, China. [6]State Key Laboratory of Environmental Chemistry and Ecotoxicology, Research Center for Eco-Environmental Sciences, Chinese Academy of Sciences, Beijing 100085, China. [7]Tsinghua Institute of Multidisciplinary Biomedical Research, Tsinghua University, Beijing 102206, China.
*These authors contributed equally to this work.
†Corresponding author. Email: ygyang@big.ac.cn (Y.-G.Y.); zhangerquan@nibs.ac.cn (E.E.Z.); huangniu@nibs.ac.cn (N. Huang)

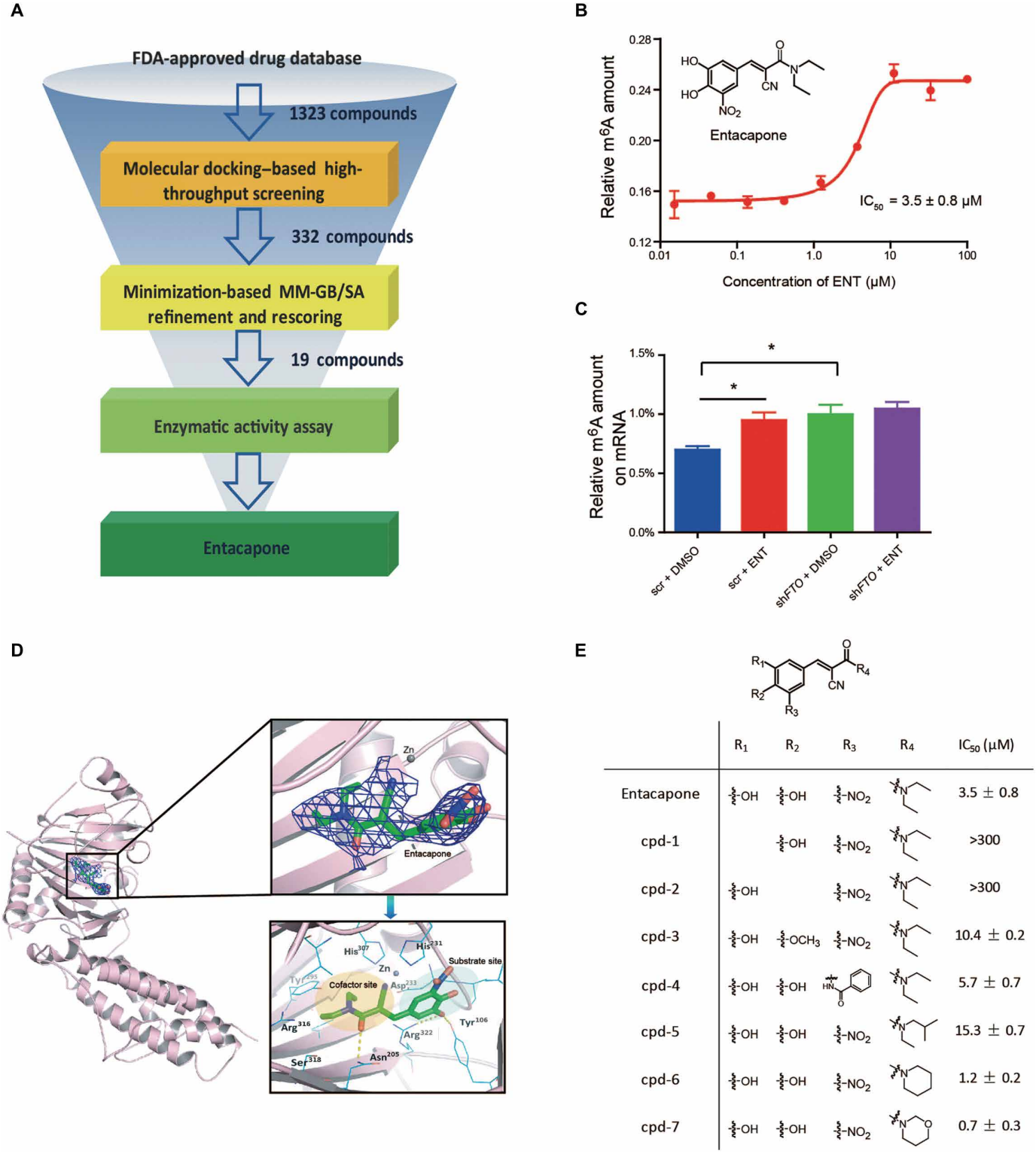

Fig. 1. Structure-based hierarchical virtual screening and hit validation. (**A**) Flowchart of structure-based virtual screening. (**B**) Enzymatic inhibition of FTO by entacapone (ENT), measured by changes in relative m^6A amount (three independent replicates). (**C**) Relative m^6A amount on mRNA in wild-type and *FTO* knockdown Hep-G2 cells with or without entacapone treatment (50 μM, 48 hours; $n = 5$ for each). scr, scramble; DMSO, dimethyl sulfoxide; sh*FTO*, *FTO* knockdown by short hairpin RNA. (**D**) Left: The global structure of the FTO-entacapone complex (pink ribbons). Top right: The electrodensity map (blue) of entacapone (sticks; carbon atoms colored in green) in the FTO active site. Bottom right: The FTO-entacapone interactions, where carbon atoms of binding site residues are colored in cyan and the hydrogen bonds are illustrated with yellow dashed lines. (**E**) Structure-activity relationship of entacapone derivatives (three independent replicates). R groups are different chemical substitutions. Data are presented as means ± SEM. cpd, compound. *$P < 0.05$.

FTO cofactor α-KG (Fig. 1B and fig. S1A) and bound to FTO with a disassociation constant of 234 nM in the presence of Fe^{2+} or 1072 nM without Fe^{2+} (fig. S1B). Consistent with the effect of *FTO* knockdown, entacapone treatment also enhanced the amount of m^6A on mRNA in a variety of human cell lines, including Hep-G2 (Fig. 1C and fig. S1C). Entacapone did not show any inhibitory effect on the enzymatic activity of the RNA m^6A demethylase AlkB homolog 5 (ALKBH5) or the ten-eleven translocation methylcytosine dioxygenase 1 (TET1), nor did it alter the DNA methylation or histone methylation patterns in entacapone-treated Hep-G2 cells (fig. S1, D to G).

The structural basis of FTO inhibition

Entacapone is structurally distinct from any known inhibitors of FTO (fig. S2, A and B). To determine the structural basis of entacapone in FTO inhibition, we determined the crystal structure of the FTO protein bound with entacapone in the presence of a Zn^{2+} ion [Protein Data Bank (PDB) code, 6AK4; Fig. 1D and table S1]. The docking pose for entacapone agreed well with the crystallographically determined binding pose (fig. S2B). Consistent with the results of our enzyme kinetic observations, entacapone occupied both the cofactor and the substrate binding sites of FTO (Fig. 1D). The metaposition hydroxyl group on the nitrocatechol ring formed hydrogen bound to Arg^{322} and Tyr^{106} at the substrate binding site. The nitrile group formed a chelation interaction with the Zn^{2+} ion, which was also evident in a recently published protein-ligand complex structure of histone demethylase (*38*). The carbonyl group formed a hydrogen bond with Asn^{205}, whereas the flexible diethyl-propanamide tail was deeply buried inside the cofactor binding site.

We performed a proof-of-concept structure-activity relationship exploration, the results of which accorded with the crystallographically determined binding mode of entacapone (Fig. 1E). Specifically, removing either of the hydroxyl groups (cpd-1 or cpd-2) diminished entacapone's enzymatic inhibitory activity, and substitution of the methoxyl group for the ortho-hydroxyl group (cpd-3) reduced inhibitory activity (IC_{50} value of 10.4 μM). Replacing the nitro group with a benzoyl-amide group (cpd-4) did not reduce the inhibitory activity (IC_{50} value of 5.7 μM), consistent with the solvent-exposed nitro group lacking direct interactions with the protein in the crystal structure. Inside the cofactor binding site, the addition of hydrophobic methyl groups on the diethyl moiety (cpd-5) reduced inhibitory activity (IC_{50} value of 15.3 μM), and rigidifying the flexible diethyl tail to alicyclic groups (cpd-6 and cpd-7) improved inhibitory activity (IC_{50} values of 1.2 and 0.7 μM, respectively). We further obtained the crystal structure of cpd-7 bound with FTO (PDB code, 6AEJ), which revealed highly similar binding poses for both cpd-7 and entacapone (fig. S2C and table S1).

The metabolic effects of entacapone

The assumed association between FTO and metabolic disorders, as well as the extensive safe history of entacapone in long-term clinical use, prompted us to evaluate the possibility of repurposing entacapone for the treatment of metabolic disorders such as obesity and diabetes. We examined the dose-response effect of entacapone in reducing body weight in a high-fat diet-induced obese (DIO) mouse model for 5 weeks (fig. S3). An effective dosing regimen (600 mg/kg of body weight blended in with food) was used throughout the rest of the animal studies. After 3 weeks of entacapone treatment, mouse body weight decreased by 10.1% compared to controls (Fig. 2A), although both groups showed similar food intake (Fig. 2B). Both fat mass and fat mass ratio were also reduced after entacapone treatment (Fig. 2C). We conducted respiration calorimetry analysis to measure the effects of entacapone on energy metabolism. Entacapone treatment increased the energy expenditure of mice (Fig. 2D). Analysis of plasma showed that entacapone caused reductions in total cholesterol (17.6%), low-density lipoprotein cholesterol (31.0%), and triglycerides (10.2%; Fig. 2E). Further, we observed that the temperature of the skin surrounding inguinal white adipose tissue (iWAT) and interscapular brown adipose tissue (BAT) was higher in entacapone-treated mice versus controls after only 3 weeks of entacapone treatment, which suggested that thermogenesis in adipose tissue was a possible cause of the increased energy expenditure observed in the entacapone-treated mice (Fig. 2, F and G).

We also found that entacapone treatment decreased fasting blood glucose in DIO mice (Fig. 2H). We subsequently used a diabetic *db/db* mouse model to evaluate these effects. As expected, entacapone-treated *db/db* mice had decreased fasting blood glucose (Fig. 2I) and improved glucose tolerance (Fig. 2J) compared to the control mice. These observations suggested that FTO inhibition may interfere with gluconeogenesis. To test this hypothesis, we generated liver-specific *Fto* knockout mice (fig. S4, A to D), which, compared to controls, showed no difference in body weight, hepatic glycogen concentration, or the concentration of two liver transaminases in serum commonly used to assess liver injury (fig. S4, E to G). However, the fasting blood glucose in liver-specific *Fto* knockout mice was lower than that of controls. We also observed the improved glucose tolerance (Fig. 2, K and L, and fig. S4H). In particular, liver-specific *Fto* knockdown mice did not show altered serum insulin concentrations, although they had reduced fasting blood glucose and an improved pyruvate tolerance (fig. S5, A to C). Thus, we provided evidence that hepatic *FTO* regulates gluconeogenesis in the liver.

FOXO1 mRNA as a direct substrate of FTO

To explore the molecular mechanism responsible for hepatic FTO-regulated gluconeogenesis, we analyzed transcriptome profiles in *FTO* knockdown Hep-G2 hepatic cells by RNA sequencing (RNA-seq). Genes differentially expressed between control and *FTO* knockdown samples were identified with fold-change cutoff value of 1.5 and the false discovery rate cutoff value of 0.001. Among the genes down-regulated after *FTO* knockdown, pathways associated with glucose metabolism, including the glycolysis/gluconeogenesis pathways, were enriched (Fig. 3A and fig. S6A). We confirmed that two critical gluconeogenic genes, glucose 6-phosphatase (*G6PC*) and phosphoenolpyruvate carboxykinase 1 (*PCK1*), were down-regulated after *FTO* knockdown (Fig. 3B and fig. S6B). Consistent with the above findings, *G6PC* was also down-regulated in entacapone-treated Hep-G2 cells (fig. S6C). Expression of these two gluconeogenic genes has been reported to be regulated by a common transcription factor, FOXO1 (*39*).

Among the m^6A sites identified in the human and mouse transcriptomes, four common sites were found in *FOXO1* mRNA (*20*). Because FTO is an m^6A demethylase, we measured the m^6A amounts of these four putative sites in FTO pulldown mRNA from Hep-G2 cells and found that two sites (m^6A-1 and m^6A-2) in *FOXO1* mRNA were strongly enriched compared to control (Fig. 3C). Consistently, synthetic mRNA fragments containing these two m^6A sites with flanking sequences were efficiently demethylated by FTO (Fig. 3C). An m^6A pulldown assay showed that m^6A amounts at these two m^6A sites in *FOXO1* mRNA were higher in *FTO* knockout cells than that

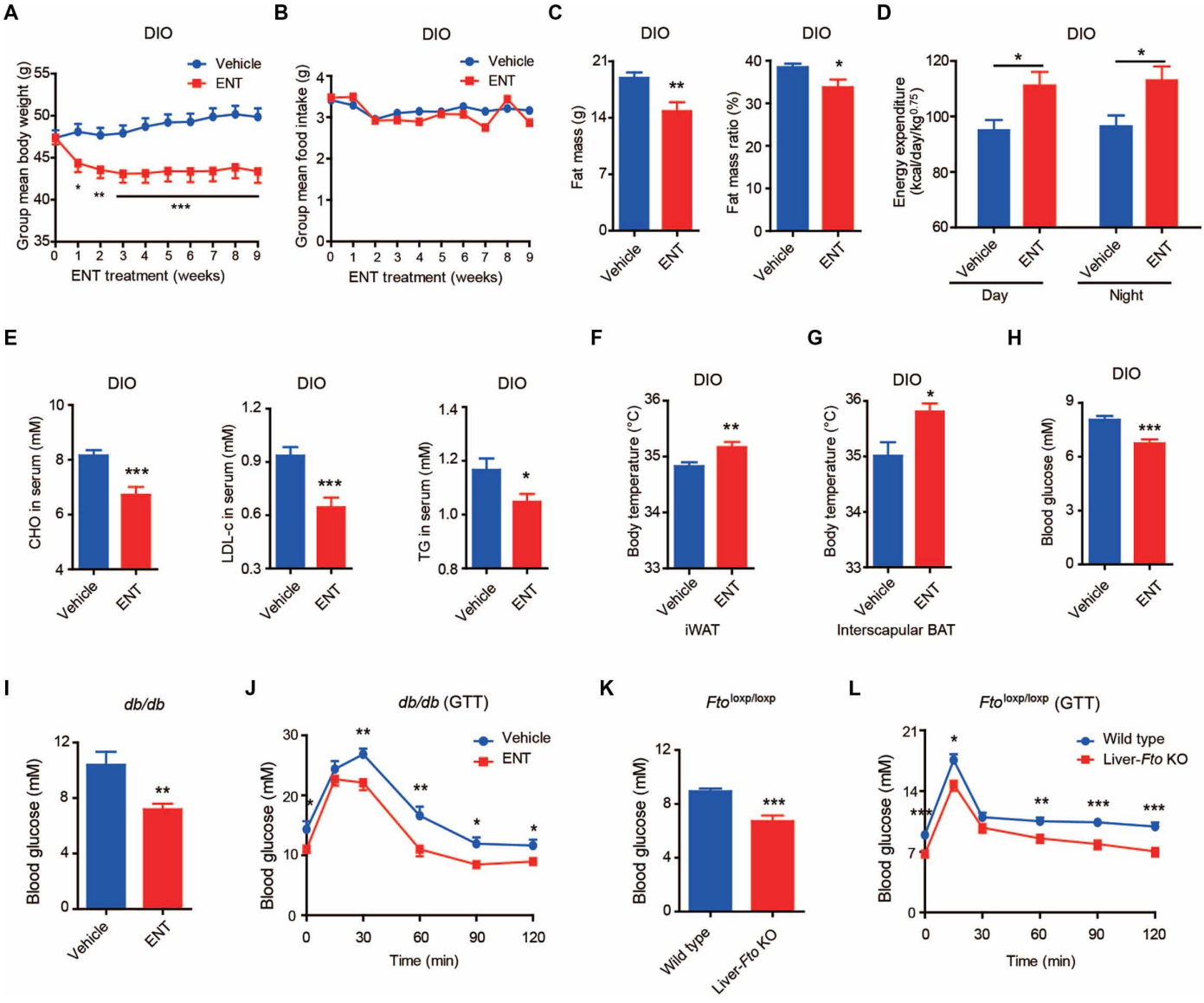

Fig. 2. Metabolic effects of entacapone treatment or *Fto* knockout. (**A** to **C**) The effects of entacapone on the (A) body weight, (B) food intake amounts, and (C) fat mass and fat mass ratio of DIO mice ($n = 10$ per group) after entacapone treatment (600 mg/kg per day) for 9 weeks. (**D**) The energy expenditure of DIO mice ($n = 8$ per group) after entacapone treatment for 9 weeks. (**E**) Total cholesterol (CHO), low-density lipoprotein cholesterol (LDL-c), and triglycerides (TG) in the serum of DIO mice ($n = 8$ for each) after entacapone treatment for 9 weeks. (**F** and **G**) The body temperature of the skin surrounding iWAT (F) and interscapular BAT (G) of DIO mice ($n = 10$ for each) after entacapone treatment for 3 weeks. (**H**) The fasting blood glucose concentrations of DIO mice ($n = 10$ for each) after entacapone treatment for 3 weeks. (**I** and **J**) The effects of entacapone on (I) the fasting blood glucose and (J) glucose tolerance test (GTT) of *db/db* mice ($n = 11$ for each) after entacapone treatment for 3 weeks. (**K** and **L**) The (K) fasting blood glucose and (L) glucose tolerance test of the hepatic *Fto* knockout (KO) mice ($n = 10$ for each). Data are presented as means ± SEM. $^*P < 0.05$, $^{**}P < 0.01$, and $^{***}P < 0.005$.

in *FTO* wild-type cells (fig. S6D). Reconstitution of *FTO* expression in *FTO* knockout cells led to the recovery of FOXO1 expression, validating the finding that FOXO1 is a downstream target of *FTO* (Fig. 3D). In line with the finding that m^{6}A modification participates in the regulation of gene translation (*22*, *24*), we observed that FTO deficiency caused by either *FTO* knockdown or treatment with entacapone led to reduced expression of FOXO1 (fig. S6E). However, FOXO1 protein expression was not affected by knocking down another m^{6}A demethylase family member, ALKBH5 (fig. S6F). These observations support the view that FTO specifically regulates FOXO1 expression by demethylating m^{6}A sites on *FOXO1* mRNA in hepatic cells.

An *FTO-FOXO1* axis regulating gluconeogenesis

Considering the central role of *FOXO1* in regulating hepatic gluconeogenesis in the fasting state (*39*–*43*), we speculated that *FOXO1* is involved in hepatic *FTO*-regulated gluconeogenesis in vivo. We evaluated the regulatory role of the *FTO-FOXO1* axis in diabetic *db/db*

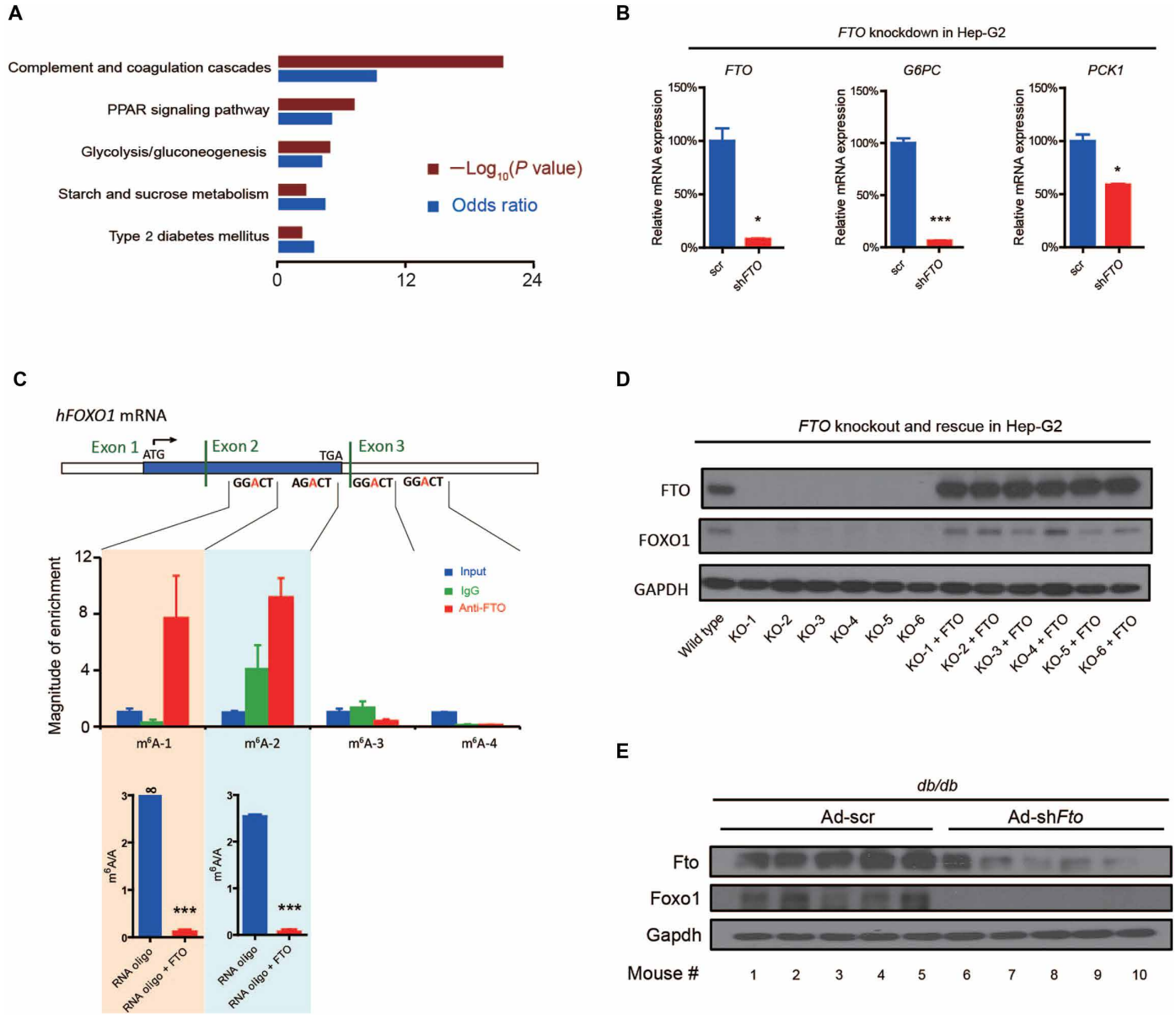

Fig. 3. Identification of *FOXO1* mRNA as a direct substrate of FTO. (**A**) The top five ranked pathways based on Kyoto Encyclopedia of Genes and Genomes (KEGG) analysis of down-regulated genes after *FTO* knockdown in the Hep-G2 cell line. PPAR, peroxisome proliferator–activated receptor. (**B**) Quantitative polymerase chain reaction analysis of the expression of *FTO*, *G6PC*, and *PCK1* after *FTO* knockdown ($n = 3$ for each), relative to actin. (**C**) The enrichment of four mammalian-conserved m^6A sites in *FOXO1* mRNA using RNA immunoprecipitation in cells ($n = 3$ for each) relative to input and the demethylation activity of FTO on the synthetic mRNA fragments containing enriched sites (three independent replicates). IgG, immunoglobulin G. (**D**) FOXO1 expression in the *FTO* knockout and *FTO* rescue cells. GAPDH, glyceraldehyde phosphate dehydrogenase. (**E**) Hepatic Foxo1 expression in adenovirally hepatic *Fto* knockdown *db/db* mice (Ad-sh*Fto*) and scramble (Ad-scr) as control ($n = 5$ for each). Data are presented as means ± SEM. $^*P < 0.05$ and $^{***}P < 0.005$.

mice. We found that *db/db* mice with *Fto* expression knocked down specifically in the liver manifested decreased fasting blood glucose concentrations and decreased expression of both Foxo1 and *G6pc* compared to control mice (Fig. 3E and fig. S7, A and B). The cyclic adenosine 3′,5′-monophosphate response element–binding protein (Creb) has been reported to transcriptionally regulate Foxo1 (*39*). However, we observed no changes in Creb expression after *Fto* knockdown (fig. S7C), indicating that it is not involved in the regulation of the *FTO-FOXO1* signaling pathway. Nor did we find any difference in the expression of *Irx3* (fig. S7D), suggesting that *Irx3* does not play a critical role in Fto-associated gluconeogenesis.

We used a live imaging system with an adenovirus-encoded *G6pc* luciferase reporter to study the *FTO-FOXO1* axis in regulating gluconeogenesis in the liver (*40*, *44*). We observed that *Fto* deficiency in mice caused by specific *Fto* knockout in the liver, expression of a catalytically dead FTO mutant (R96A), or inhibition of Fto activity by entacapone led to a reduction in the G6pc luciferase signal. We observed a similar phenomenon in mice with a liver-specific *Foxo1*

knockout (Fig. 4A and fig. S7E). We next determined whether entacapone regulated liver gluconeogenesis via the *FTO-FOXO1* axis in an m^6A-dependent manner. In entacapone-treated hepatic *Foxo1* knockout mice, only mice adenovirally reexpressing wild-type *Foxo1* (liver-*Foxo1*-KO + Ad-WT-*Foxo1*), but not synonymously m^6A-mutated *Foxo1* (liver-*Foxo1*-KO + Ad-mut-*Foxo1*), showed a reduction in both fasting blood glucose and liver-specific G6pc luciferase signal (Fig. 4B). These findings confirmed that the *FTO-FOXO1* axis regulates hepatic gluconeogenesis and that entacapone regulates fasting blood glucose through its direct effect on the hepatic *FTO-FOXO1* signaling axis.

An *FTO-FOXO1* axis modulating thermogenesis

We wished to determine the molecular mechanisms by which *FTO-FOXO1* regulated thermogenesis in adipose tissues of entacapone-treated DIO mice. Histological analysis revealed that entacapone treatment decreased cell size in murine iWAT (Fig. 5A). RNA-seq analysis of iWAT from entacapone-treated and control mice showed that entacapone treatment resulted in a >10-fold increase in the expression of *Ucp1* (Fig. 5B), a well-known biomarker of the thermogenesic state of adipose tissues (*45*–*48*). The oxidative phosphorylation pathway was strongly enriched among the genes up-regulated by entacapone (Fig. 5C), including many components of complexes I to V of the electron transport chain (fig. S8A). These observations suggested that the antiobesity effect of Fto inhibition by entacapone in DIO mice may have resulted from increased thermogenesis in adipose tissue.

We found that the overall extent of m^6A methylation in the iWAT of entacapone-treated mice was 21.0% higher than in control mice (Fig. 5D). We established the m^6A methylomes of iWAT from control and entacapone-treated mice using an m^6A antibody pulldown assay combined with m^6A seq. In both control and entacapone-treated samples, m^6A peaks were enriched in an RGACH motif (fig. S8B), which mostly occurred in high abundance in mRNA coding sequences, especially near stop codons, and 3′UTRs (Fig. 5E and fig. S8, C and D). However, entacapone treatment led to both enhanced and newly appearing m^6A peaks that were enriched in the Foxo pathway (fig. S8, E and F). Specifically, m^6A-1, the first m^6A site located in the coding sequence of *FOXO1* mRNA in Hep-G2 cells, was uniquely present in the iWAT of entacapone-treated DIO mice. We also observed an increased m^6A peak at m^6A-2 site of *Foxo1* mRNA, the second m^6A site identified in the *FOXO1* coding sequence (CDS) of Hep-G2 cells (Fig. 5F). Both m^6A peaks were enriched upon Fto inhibition by entacapone, which we confirmed by m^6A antibody pulldown combined with quantitative polymerase chain reaction assays (Fig. 5G). m^6A peaks were not detected on *Ucp1* mRNA in iWAT of either entacapone-treated or control mouse samples, indicating that *Ucp1* mRNA is not a direct substrate of Fto (fig. S8G).

Because FOXO1 has been shown to repress the *UCP1* gene transcription (*49*, *50*), we analyzed the effect of entacapone on Fto, Foxo1, and Ucp1 expression in iWAT of DIO mice. In accordance with suppressed Fto activity after entacapone treatment, we observed decreased Foxo1 expression and increased Ucp1 expression in iWAT (Fig. 5H); similar effects were also evident in interscapular BAT, with

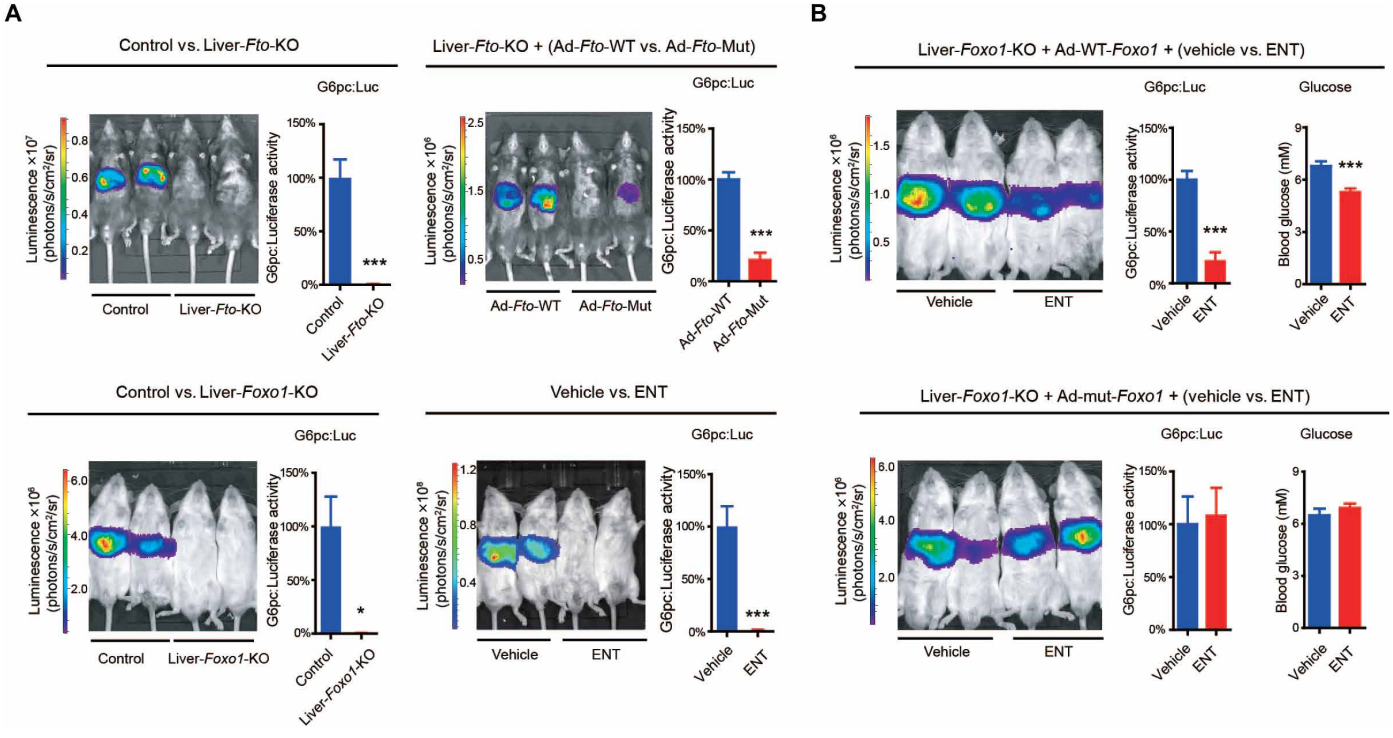

Fig. 4. The *FTO-FOXO1-G6PC* signaling cascade and gluconeogenesis in liver. (**A**) The effects on *G6pc*–luciferase (Luc) signal of hepatic *Fto* knockout (liver-*Fto*-KO and control; $n = 6$ for each), *FTO* loss-of-function mutation (R96A) (Ad-*Fto*-Mut and Ad-*Fto*-WT; $n = 10$ for each), *Foxo1* knockout (liver-*Foxo1*-KO; $n = 6$ for each), or pharmacological attenuation of Fto activity via administration of entacapone (600 mg/kg per day) for 11 days (vehicle; $n = 6$ for each). (**B**) The effects of entacapone treatment on the G6pc:Luciferase signal and the fasting blood glucose in hepatic *Foxo1* knockout mice expressing wild-type *Foxo1* ($n = 6$ for each) and in hepatic *Foxo1* knockout mice expressing synonymous mutant *Foxo1* ($n = 5$ for each). Data are presented as means ± SEM. $^*P < 0.05$ and $^{***}P < 0.005$.

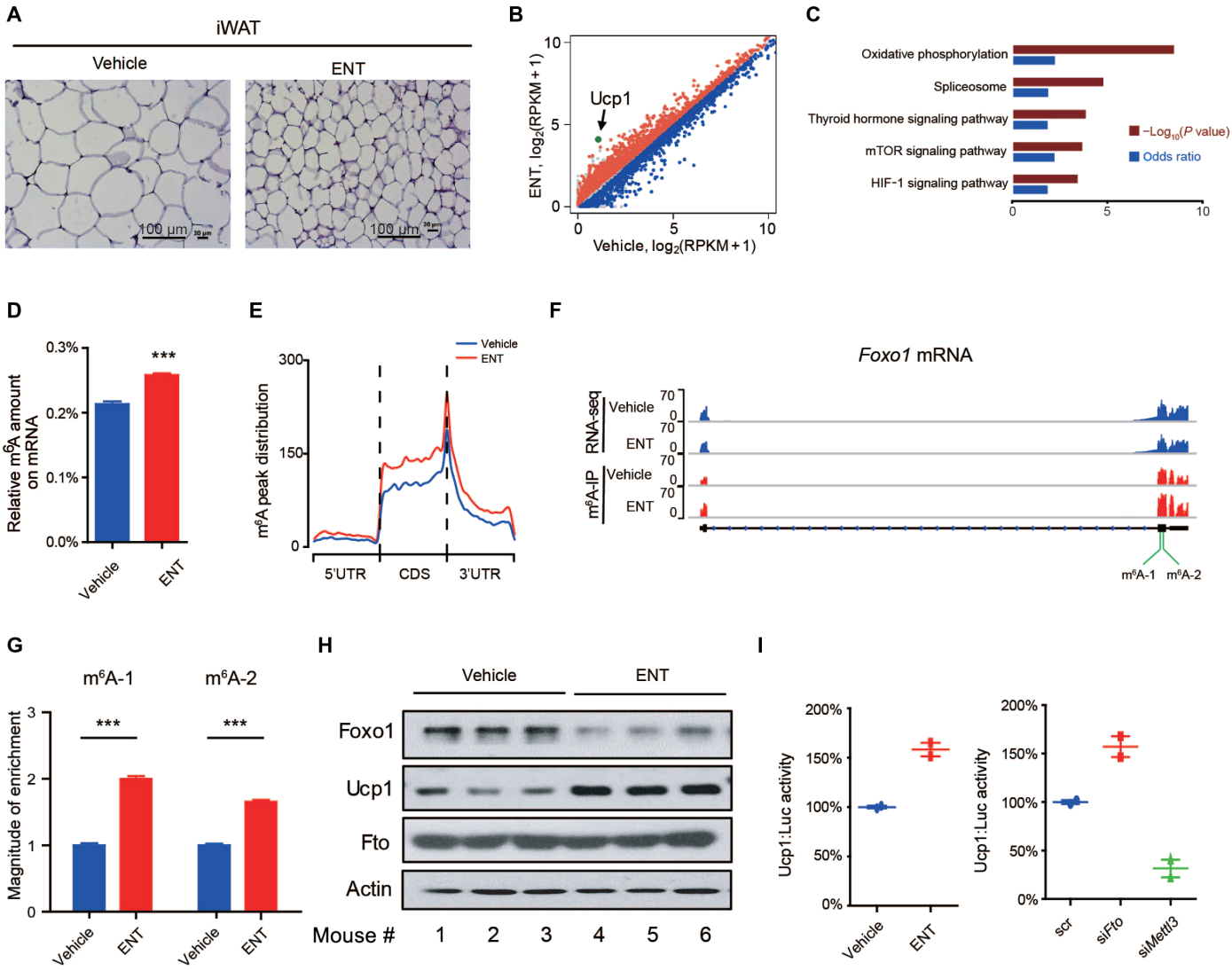

Fig. 5. The *FTO-FOXO1-UCP1* regulation of thermogenesis in adipose tissue. (**A**) Adipocyte cell sizes of iWAT in DIO mice (hematoxylin and eosin staining, 200×). (**B**) Scatter plot of RNA-seq analysis of iWAT (entacapone versus vehicle). RPKM, reads per kilo base of exon model per million mapped reads. (**C**) Representative KEGG pathways enriched in the up-regulated genes were identified using RNA-seq analysis. HIF-1, hypoxia-inducible factor–1. (**D**) Relative m^{6}A amounts on mRNA of iWAT in DIO mice ($n = 3$ for each). (**E**) Distribution of m^{6}A peaks across the length of mRNA transcripts. 5′ untranslated region (5′UTRs), CDSs, and 3′UTRs of mRNAs were individually binned into regions spanning 1% of their total length, and the percentage of m^{6}A peaks that fall within each bin was determined. The moving averages of peak percentage in iWAT of vehicle-treated and entacapone-treated mice are shown. (**F**) The Integrative Genomics Viewer tracks displaying RNA-seq and m^{6}A sequencing (m^{6}A-seq) read distribution for the *Foxo1* mRNA of iWAT. IP, immunoprecipitation. (**G**) Enrichment of m^{6}A-1 and m^{6}A-2 sites on *Foxo1* mRNA in the iWAT of DIO mice ($n = 3$ for each). (**H**) Western blot analysis of Foxo1, Ucp1, and Fto expression in iWAT of DIO mice. (**I**) Ucp1:Luciferase signals of entacapone treatment and *Fto* and *Mettl3* knockdown by small interfering RNA (si*Fto* and si*Mettl3*, respectively) in 293T cells ($n = 2$ for each). Data are presented as means ± SEM. ***$P < 0.005$.

decreased Foxo1 and increased Ucp1 expression observed after entacapone treatment (fig. S8, H and I). We then used a cell-based Ucp1-luciferase reporter assay to examine the role of *FTO-FOXO1* signaling in controlling *Ucp1* gene transcription. *Fto* inhibition by either entacapone treatment or knockdown enhanced *Ucp1* promoter activity. Conversely, knockdown of *Mettl3*, a methyltransferase with the opposite role of *Fto*, markedly suppressed *Ucp1* promoter activity (Fig. 5I). Thus, the *FTO-FOXO1* axis is implicated in the regulation of thermogenesis in the adipose tissues through control of transcription of *FOXO1* downstream targets such as *UCP1*.

We generated *Foxo1* mutant mice by synonymously mutating the m^{6}A-2 site on *Foxo1* mRNA (*Foxo1*-Mut) to further confirm the role of the *FTO-FOXO1* axis in vivo (fig. S9, A to C). We first performed RNA-seq on the liver samples taken from fasted hepatic *Fto* knockout and *Foxo1*-Mut mice. Many of the commonly down-regulated genes in these mice mutants are known to be involved in metabolism-related pathways including gluconeogenesis (fig. S9, D and E). Entacapone treatment for 3 weeks led to a reduction in both body weight and fasting blood glucose concentration in wild-type mice but not in *Foxo1*-Mut mice (fig. S9, F and G). In addition, entacapone treatment did not influence the food intake of either *Foxo1* wild-type or *Foxo1*-Mut mice (fig. S9H). These results demonstrated that entacapone regulates body weight and blood glucose through *FTO-FOXO1* signaling in vivo (fig. S10).

DISCUSSION

Despite long-standing research efforts, the discovery of therapeutic interventions that can regulate metabolic homeostasis proceeds slowly. We selected the m^6A demethylase FTO as a potential target and performed a computer-aided virtual screening to find small molecular inhibitors of FTO. We identified entacapone, an FDA-approved drug, as a selective inhibitor of FTO activity involved in the regulation of metabolic homeostasis. The pharmaceutical drug entacapone could serve as a useful "tool compound" to study the in vivo functions of FTO. Furthermore, the binding characteristics of our solved FTO-entacapone crystal complex structure and our proof-of-concept structure-activity relationship study establish a structural foundation for designing a new generation of drug-like FTO inhibitors. Our strategy moving from virtual screening to hit validation and from animal physiology to mechanistic elucidation represents an illustrative model potentially valuable for the next generation of translational medicine.

Entacapone was originally approved by the FDA for use as an adjunctive therapy in combination with levodopa and carbidopa for the treatment of Parkinson's disease. Mechanistically, entacapone is believed to peripherally inhibit COMT activity, increasing the bioavailability of levodopa and extending its duration of action in the brain (*32*). We cannot completely exclude the effects of entacapone on COMT from its demonstrated effects on FTO. However, it was reported that there was no significant difference in mean body weight between *COMT* knockout and wild-type mice in different age groups (*51*, *52*). In addition, COMT deficiencies in DIO mice (by use of a COMT inhibitor or small interfering RNA), or from a low-activity COMT allele in humans, have been implicated in exacerbated characteristics of type 2 diabetes and obesity (*53*, *54*). Therefore, we reasoned that the metabolic effects of entacapone strongly implicate the engagement of FTO.

Our identification of *FOXO1* mRNA as a substrate of FTO may aid the discovery of biomarkers for *FTO*-associated diseases. FOXO1 is a transcription factor, and FOXO1 has been traditionally considered to be a difficult target for manipulation through pharmacological approaches (*43*). Selectively silencing FOXO1 through the inhibition of FTO could potentially be used to treat dysregulated metabolic homeostasis.

Considering that *FOXO1* mRNA is not the only direct substrate of FTO, it is likely that other FTO target genes may have functional roles related to obesity or diabetes. It was reported that an m^6A_m site at the 5′ cap of mRNA molecules is a substrate of FTO and FTO-mediated demethylation of this site reduces mRNA stability (*19*). However, our RNA-seq results only illustrated the presence of specific internal m^6A sites within *FOXO1* mRNA. *FOXO1* mRNA stability is not changed by *FTO* expression knockdown or activity inhibition. In particular, synonymously mutating this specific m^6A site effectively blocked the effects of *FTO-FOXO1* axis. Therefore, the internal m^6A site identified in our study is critical in mediating the regulatory role of *FTO-FOXO1* axis both in thermogenesis in adipose tissues and in gluconeogenesis in the liver.

Our study has several limitations. We are aware that data obtained from rodent models cannot be extrapolated directly to humans, especially given the differences in adipose tissue metabolism between mice and humans (*55*, *56*). Further studies will be needed to establish relevant efficacies in human cells and tissues. Another limitation was the potentially problematic high dose of entacapone required in our animal studies, on account of its low potency and its short plasma elimination half-life (about 0.5 hours); we thus conclude that it is desirable to develop entacapone analogs with improved pharmacokinetic and pharmacodynamic properties for the treatment of metabolic disorders.

MATERIALS AND METHODS

Study design

The aims of this study were to identify potential FTO inhibitors from FDA-approved drugs by applying a structure-based hierarchical virtual screening strategy and to study the molecular mechanism of the regulatory role of FTO in metabolism. The enzymatic inhibitory activity of the selected compounds was measured using an FTO-catalyzed demethylation assay. The binding affinity of entacapone against FTO was measured, and the complex structures of FTO bound with inhibitors were determined to elucidate the protein-ligand interactions. We synthesized analogs of entacapone to explore a proof-of-concept structure-activity relationship. To evaluate the possibility of repurposing entacapone for the treatment of FTO-related metabolic disorders such as obesity and diabetes, we measured the therapeutic efficacy of entacapone in DIO and diabetic mouse models. Transcriptome sequencing analysis of FTO knockout hepatic cells and entacapone-treated adipocytes identified substrates of FTO. We confirmed the *FTO-FOXO1* regulatory axis using live-imaging analysis. All procedures in this protocol were conducted with the approval of the Institutional Animal Care and Use Committee of the National Institute of Biological Sciences, Beijing in accordance with the governmental regulations of China. Animals were randomized into groups with similar body weights or similar blood glucose concentrations before study initiation. Investigators and data analyzers were blinded for the mouse studies. Outliers were excluded from a group if they were located ±2 SDs away from the group mean. Sample sizes were determined by internal pilot studies and are listed in the figure legends. All experiments were replicated more than once, as indicated in figure legends.

Animal experiments

Wild-type mice were purchased from the Beijing Vital River Laboratory Animal Technology Co. Ltd. The *db/db* mice were purchased from the Nanjing Biomedical Research Institute of Nanjing University; these were introduced from the Jackson Laboratory. The albumin-cre mice and the $Foxo1^{loxp/loxp}$ mice were obtained from the Jackson Laboratory. Animals were maintained in a 12-hour light/dark photoperiod with food and water provided ad libitum.

Structure-based hierarchical virtual screening

We applied a structure-based hierarchical virtual screening strategy to identify potential FTO inhibitors from a library of FDA-approved drugs. Briefly, an automatic docking procedure was applied to generate ligand binding poses, as described previously (*36*). The binding site was defined as both the substrate site and the cofactor *N*-oxalylglycine site, as in the crystal structure of FTO (PDB code, 3LFM) (*17*). The Fe^{2+} ion was processed according to a previously published protocol (*57*), with reduced van der Waals interaction and partial atomic charge parameters. We docked 1323 FDA-approved drugs processed by ZINC (*58*) against FTO using DOCK 3.5.54 (*59*–*61*) and outputted the top 500 docking poses for each compound. We filtered these docking poses based on three predefined structural

descriptors according to the FTO crystal complex structure bound with N3-methylthymidine. First, the docked compounds should form close atomic contacts (i.e., distance cutoff of 4.5 Å) with residues in both the substrate binding site (including Arg^{322}, Arg^{96}, and Tyr^{106}) and the cofactor binding pocket (including Tyr^{295}, Arg^{316}, Ser^{318}, and Asn^{205}). Second, the qualified ligands should form at least one hydrogen bond interaction (distance threshold of 4.5 Å) with the oxygen atom of the hydroxyl group of Tyr^{106} and the nitrogen atom of the amino group of Glu^{234}. Third, the desired candidates should form chelation interactions with the Fe^{2+} (distance cutoff of 3 Å with acceptor heteroatoms). After filtering, 332 compounds remained. The docking poses were then minimized and rescored with a more sophisticated scoring method Molecular Mechanics/Generalized Born Surface Area using the PLOP program (*34*). The refined poses were filtered and visually checked, and 19 compounds were selected for further experimental validation (table S2).

Phenotypic measurement

Because entacapone is rapidly metabolized in vivo (*32*), we optimized the route of administration and dosage of entacapone. For the treatment group, entacapone (600 mg/kg of body weight) was orally administered to the mice by blending it with the food. The measured plasma concentration of entacapone in mice (averaged for an entire 24-hour period) was 6.4 ± 0.8 μM.

Counter-obesity experiments were performed in a DIO mice model. Eight-week-old male C57BL/6 mice were fed a high-fat diet (45% fat; OpenSource Diets) for 12 weeks. Obese mice with body weight 20% higher than that of mice fed a normal diet were selected for experiments. Entacapone was administered to 10 randomly selected obese mice, with vehicle-treated mice as controls. Body mass and food intake amount were measured each week. The body composition of live mice was determined using the magnetic resonance imaging analyzer (EchoMRI-700). Oxygen consumption, carbon dioxide production, and respiratory exchange ratio were measured by Physiocage (Oxylet, Panlab). After 24 hours of acclimatization, calorimetry parameters were measured for 24 hours. Body temperature of the skin surrounding iWAT and interscapular BAT was measured using infRec analyzer (NS9500 Lite, Avio/NEC) after entacapone treatment for 3 weeks. Sections of iWAT and interscapular BAT were counterstained with hematoxylin.

Blood samples were extracted from the tail and examined with an Aviva Nano blood glucose meter system (Accu-Chek). For the glucose tolerance tests and the pyruvate tolerance tests, mice were injected intraperitoneally with glucose (2 g/kg of body weight; Sigma-Aldrich) or pyruvate (2 g/kg of body weight; Sigma-Aldrich) after fasting for 6 hours. Blood glucose was measured 0, 15, 30, 60, 90, and 120 min after injection. Hepatic glycogen was measured with a Glycogen Assay Kit (Abcam). Cholesterol, low-density lipoprotein cholesterol, triglycerides, serum glutamic oxaloacetic transaminase (SGOT), and serum glutamic pyruvic transaminase (SGPT) in serum were measured with a Hitachi Biochemical Analyzer. Serum insulin was measured with an enzyme-linked immunosorbent assay kit (Millipore).

Statistical analysis

Data in figures are shown as means ± SEM. Normality tests were conducted before unpaired two-tailed Student's *t* tests in all animal studies. $P < 0.05$ was considered statistically significant. $^{*}P < 0.05$, $^{**}P < 0.01$, and $^{***}P < 0.005$. All data values are reported in data file S1.

SUPPLEMENTARY MATERIALS

stm.sciencemag.org/cgi/content/full/11/488/eaau7116/DC1

Materials and Methods

Fig. S1. Experimental validation of the FTO-entacapone interaction and entacapone target selectivity assessment.

Fig. S2. Crystal complex structures of FTO bound with different types of inhibitors.

Fig. S3. Dose-response effect of entacapone on the body weight of DIO mice.

Fig. S4. Generation and phenotypic measurements of liver-specific *Fto* knockout mice.

Fig. S5. Hepatic *Fto* regulates gluconeogenesis in the liver.

Fig. S6. *FTO-FOXO1* regulatory axis modulates *G6PC* and *PCK1* expression in a hepatic cell line.

Fig. S7. Hepatic *Fto* knockdown in *db/db* mice and enzymatic activity of FTO R96A mutant protein.

Fig. S8. Characterization of m^6A modifications and changes in gene expression in mouse adipose tissues.

Fig. S9. Generation, RNA-seq analysis, and phenotypic analysis of *Foxo1*-Mut mice with the *Foxo1* synonymous mutation at the *Foxo1*–m^6A-2 site.

Fig. S10. Proposed *FTO-FOXO1* regulatory axis in adipose tissue and liver.

Table S1. Statistics on data collection and structure refinement of FTO-inhibitor complex structures.

Table S2. Structures and FTO enzymatic inhibition activities of 19 selected compounds from virtual screening.

Data file S1. Summary of all reported data values.

References (*62*–*78*)

REFERENCES AND NOTES

1. C. Dina, D. Meyre, S. Gallina, E. Durand, A. Körner, P. Jacobson, L. M. Carlsson, W. Kiess, V. Vatin, C. Lecoeur, J. Delplanque, E. Vaillant, F. Pattou, J. Ruiz, J. Weill, C. Levy-Marchal, F. Horber, N. Potoczna, S. Hercberg, C. Le Stunff, P. Bougnères, P. Kovacs, M. Marre, B. Balkau, S. Cauchi, J. C. Chevre, P. Froguel, Variation in FTO contributes to childhood obesity and severe adult obesity. *Nat. Genet.* **39**, 724–726 (2007).
2. T. M. Frayling, N. J. Timpson, M. N. Weedon, E. Zeggini, R. M. Freathy, C. M. Lindgren, J. R. Perry, K. S. Elliott, H. Lango, N. W. Rayner, B. Shields, L. W. Harries, J. C. Barrett, S. Ellard, C. J. Groves, B. Knight, A. M. Patch, A. R. Ness, S. Ebrahim, D. A. Lawlor, S. M. Ring, Y. Ben-Shlomo, M. R. Jarvelin, U. Sovio, A. J. Bennett, D. Melzer, L. Ferrucci, R. J. Loos, I. Barroso, N. J. Wareham, F. Karpe, K. R. Owen, L. R. Cardon, M. Walker, G. A. Hitman, C. N. Palmer, A. S. Doney, A. D. Morris, G. D. Smith, A. T. Hattersley, M. I. McCarthy, A common variant in the FTO gene is associated with body mass index and predisposes to childhood and adult obesity. *Science* **316**, 889–894 (2007).
3. L. J. Scott, K. L. Mohlke, L. L. Bonnycastle, C. J. Willer, Y. Li, W. L. Duren, M. R. Erdos, H. M. Stringham, P. S. Chines, A. U. Jackson, L. Prokunina-Olsson, C. J. Ding, A. J. Swift, N. Narisu, T. Hu, R. Pruim, R. Xiao, X. Y. Li, K. N. Conneely, N. L. Riebow, A. G. Sprau, M. Tong, P. P. White, K. N. Hetrick, M. W. Barnhart, C. W. Bark, J. L. Goldstein, L. Watkins, F. Xiang, J. Saramies, T. A. Buchanan, R. M. Watanabe, T. T. Valle, L. Kinnunen, G. R. Abecasis, E. W. Pugh, K. F. Doheny, R. N. Bergman, J. Tuomilehto, F. S. Collins, M. Boehnke, A genome-wide association study of type 2 diabetes in Finns detects multiple susceptibility variants. *Science* **316**, 1341–1345 (2007).
4. A. Scuteri, S. Sanna, W. M. Chen, M. Uda, G. Albai, J. Strait, S. Najjar, R. Nagaraja, M. Orrú, G. Usala, M. Dei, S. Lai, A. Maschio, F. Busonero, A. Mulas, G. B. Ehret, A. A. Fink, A. B. Weder, R. S. Cooper, P. Galan, A. Chakravarti, D. Schlessinger, A. Cao, E. Lakatta, G. R. Abecasis, Genome-wide association scan shows genetic variants in the FTO gene are associated with obesity-related traits. *PLOS Genet.* **3**, e115 (2007).
5. J. Yang, R. J. Loos, J. E. Powell, S. E. Medland, E. K. Speliotes, D. I. Chasman, L. M. Rose, G. Thorleifsson, V. Steinthorsdottir, R. Mägi, L. Waite, A. V. Smith, L. M. Yerges-Armstrong, K. L. Monda, D. Hadley, A. Mahajan, G. Li, K. Kapur, V. Vitart, J. E. Huffman, S. R. Wang, C. Palmer, T. Esko, K. Fischer, J. H. Zhao, A. Demirkan, A. Isaacs, M. F. Feitosa, J. Luan, N. L. Heard-Costa, C. White, A. U. Jackson, M. Preuss, A. Ziegler, J. Eriksson, Z. Kutalik, F. Frau, I. M. Nolte, J. V. Van Vliet-Ostaptchouk, J. J. Hottenga, K. B. Jacobs, N. Verweij, A. Goel, C. Medina-Gomez, K. Estrada, J. L. Bragg-Gresham, S. Sanna, C. Sidore, J. Tyrer, A. Teumer, I. Prokopenko, M. Mangino, C. M. Lindgren, T. L. Assimes, A. R. Shuldiner, J. Hui, J. P. Beilby, W. L. McArdle, P. Hall, T. Haritunians, L. Zgaga, I. Kolcic, O. Polasek, T. Zemunik, B. A. Oostra, M. J. Junttila, H. Gronberg, S. Schreiber, A. Peters, A. A. Hicks, J. Stephens, N. S. Foad, J. Laitinen, A. Pouta, M. Kaakinen, G. Willemsen, J. M. Vink, S. H. Wild, G. Navis, F. W. Asselbergs, G. Homuth, U. John, C. Iribarren, T. Harris, L. Launer, V. Gudnason, J. R. O'Connell, E. Boerwinkle, G. Cadby, L. J. Palmer, A. L. James, A. W. Musk, E. Ingelsson, B. M. Psaty, J. S. Beckmann, G. Waeber, P. Vollenweider, C. Hayward, A. F. Wright, I. Rudan, L. C. Groop, A. Metspalu, K. T. Khaw, C. M. van Duijn, I. B. Borecki, M. A. Province, N. J. Wareham, J. C. Tardif, H. V. Huikuri, L. A. Cupples, L. D. Atwood, C. S. Fox, M. Boehnke, F. S. Collins, K. L. Mohlke, J. Erdmann, H. Schunkert, C. Hengstenberg, K. Stark, M. Lorentzon, C. Ohlsson, D. Cusi, J. A. Staessen, M. M. Van der Klauw, P. P. Pramstaller, S. Kathiresan, J. D. Jolley, S. Ripatti, M. R. Jarvelin, E. J. de Geus, D. I. Boomsma, B. Penninx, J. F. Wilson, H. Campbell, S. J. Chanock,

P. van der Harst, A. Hamsten, H. Watkins, A. Hofman, J. C. Witteman, M. C. Zillikens, A. G. Uitterlinden, F. Rivadeneira, L. A. Kiemeney, S. H. Vermeulen, G. R. Abecasis, D. Schlessinger, S. Schipf, M. Stumvoll, A. Tönjes, T. D. Spector, K. E. North, G. Lettre, M. I. McCarthy, S. I. Berndt, A. C. Heath, P. A. Madden, D. R. Nyholt, G. W. Montgomery, N. G. Martin, B. McKnight, D. P. Strachan, W. G. Hill, H. Snieder, P. M. Ridker, U. Thorsteinsdottir, K. Stefansson, T. M. Frayling, J. N. Hirschhorn, M. E. Goddard, P. M. Visscher, FTO genotype is associated with phenotypic variability of body mass index. *Nature* **490**, 267–272 (2012).

6. M. Claussnitzer, S. N. Dankel, K. H. Kim, G. Quon, W. Meuleman, C. Haugen, V. Glunk, I. S. Sousa, J. L. Beaudry, V. Puviindran, N. A. Abdennur, J. Liu, P. A. Svensson, Y. H. Hsu, D. J. Drucker, G. Mellgren, C. C. Hui, H. Hauner, M. Kellis, FTO obesity variant circuitry and adipocyte browning in humans. *N. Engl. J. Med.* **373**, 895–907 (2015).
7. S. Smemo, J. J. Tena, K. H. Kim, E. R. Gamazon, N. J. Sakabe, C. Gómez-Marín, I. Aneas, F. L. Credidio, D. R. Sobreira, N. F. Wasserman, J. H. Lee, V. Puviindran, D. Tam, M. Shen, J. E. Son, N. A. Vakili, H. K. Sung, S. Naranjo, R. D. Acemel, M. Manzanares, A. Nagy, N. J. Cox, C. C. Hui, J. L. Gomez-Skarmeta, M. A. Nobrega, Obesity-associated variants within FTO form long-range functional connections with IRX3. *Nature* **507**, 371–375 (2014).
8. C. Church, S. Lee, E. A. Bagg, J. S. McTaggart, R. Deacon, T. Gerken, A. Lee, L. Moir, J. Mecinovic, M. M. Quwailid, C. J. Schofield, F. M. Ashcroft, R. D. Cox, A mouse model for the metabolic effects of the human fat mass and obesity associated FTO gene. *PLOS Genet.* **5**, e1000599 (2009).
9. C. Church, L. Moir, F. McMurray, C. Girard, G. T. Banks, L. Teboul, S. Wells, J. C. Bruning, P. M. Nolan, F. M. Ashcroft, R. D. Cox, Overexpression of Fto leads to increased food intake and results in obesity. *Nat. Genet.* **42**, 1086–1092 (2010).
10. J. Fischer, L. Koch, C. Emmerling, J. Vierkotten, T. Peters, J. C. Bruning, U. Ruther, Inactivation of the Fto gene protects from obesity. *Nature* **458**, 894–898 (2009).
11. P. Gulati, M. K. Cheung, R. Antrobus, C. D. Church, H. P. Harding, Y. C. Tung, D. Rimmington, M. Ma, D. Ron, P. J. Lehner, F. M. Ashcroft, R. D. Cox, A. P. Coll, S. O'Rahilly, G. S. Yeo, Role for the obesity-related FTO gene in the cellular sensing of amino acids. *Proc. Natl. Acad. Sci. U.S.A.* **110**, 2557–2562 (2013).
12. D. Tews, P. Fischer-Posovszky, T. Fromme, M. Klingenspor, J. Fischer, U. Ruther, R. Marienfeld, T. F. Barth, P. Moller, K. M. Debatin, M. Wabitsch, FTO deficiency induces UCP-1 expression and mitochondrial uncoupling in adipocytes. *Endocrinology* **154**, 3141–3151 (2013).
13. J. R. Speakman, FTO effect on energy demand versus food intake. *Nature* **464**, E1 (2010).
14. N. J. Poritsanos, P. S. Lew, T. M. Mizuno, Relationship between blood glucose levels and hepatic Fto mRNA expression in mice. *Biochem. Biophys. Res. Commun.* **400**, 713–717 (2010).
15. A. Bravard, G. Vial, M. A. Chauvin, Y. Rouille, B. Bailleul, H. Vidal, J. Rieusset, FTO contributes to hepatic metabolism regulation through regulation of leptin action and STAT3 signalling in liver. *Cell Commun. Signal.* **12**, 4 (2014).
16. T. Gerken, C. A. Girard, Y. C. Tung, C. J. Webby, V. Saudek, K. S. Hewitson, G. S. Yeo, M. A. McDonough, S. Cunliffe, L. A. McNeill, J. Galvanovskis, P. Rorsman, P. Robins, X. Prieur, A. P. Coll, M. Ma, Z. Jovanovic, I. S. Farooqi, B. Sedgwick, I. Barroso, T. Lindahl, C. P. Ponting, F. M. Ashcroft, S. O'Rahilly, C. J. Schofield, The obesity-associated FTO gene encodes a 2-oxoglutarate-dependent nucleic acid demethylase. *Science* **318**, 1469–1472 (2007).
17. Z. Han, T. Niu, J. Chang, X. Lei, M. Zhao, Q. Wang, W. Cheng, J. Wang, Y. Feng, J. Chai, Crystal structure of the FTO protein reveals basis for its substrate specificity. *Nature* **464**, 1205–1209 (2010).
18. G. Jia, Y. Fu, X. Zhao, Q. Dai, G. Zheng, Y. Yang, C. Yi, T. Lindahl, T. Pan, Y. G. Yang, C. He, *N*6-methyladenosine in nuclear RNA is a major substrate of the obesity-associated FTO. *Nat. Chem. Biol.* **7**, 885–887 (2011).
19. J. Mauer, X. Luo, A. Blanjoie, X. Jiao, A. V. Grozhik, D. P. Patil, B. Linder, B. F. Pickering, J. J. Vasseur, Q. Chen, S. S. Gross, O. Elemento, F. Debart, M. Kiledjian, S. R. Jaffrey, Reversible methylation of m^6A_m in the 5′ cap controls mRNA stability. *Nature* **541**, 371–375 (2017).
20. D. Dominissini, S. Moshitch-Moshkovitz, S. Schwartz, M. Salmon-Divon, L. Ungar, S. Osenberg, K. Cesarkas, J. Jacob-Hirsch, N. Amariglio, M. Kupiec, R. Sorek, G. Rechavi, Topology of the human and mouse m^6A RNA methylomes revealed by m^6A-seq. *Nature* **485**, 201–206 (2012).
21. K. D. Meyer, Y. Saletore, P. Zumbo, O. Elemento, C. E. Mason, S. R. Jaffrey, Comprehensive analysis of mRNA methylation reveals enrichment in 3′ UTRs and near stop codons. *Cell* **149**, 1635–1646 (2012).
22. B. Slobodin, R. Han, V. Calderone, J. A. F. O. Vrielink, F. Loayza-Puch, R. Elkon, R. Agami, Transcription impacts the efficiency of mRNA translation via co-transcriptional N6-adenosine methylation. *Cell* **169**, 326–337.e12 (2017).
23. X. Wang, Z. Lu, A. Gomez, G. C. Hon, Y. Yue, D. Han, Y. Fu, M. Parisien, Q. Dai, G. Jia, B. Ren, T. Pan, C. He, N^6-methyladenosine-dependent regulation of messenger RNA stability. *Nature* **505**, 117–120 (2014).
24. X. Wang, B. S. Zhao, I. A. Roundtree, Z. Lu, D. Han, H. Ma, X. Weng, K. Chen, H. Shi, C. He, N^6-methyladenosine modulates messenger RNA translation efficiency. *Cell* **161**, 1388–1399 (2015).
25. X. Zhao, Y. Yang, B. F. Sun, Y. Shi, X. Yang, W. Xiao, Y. J. Hao, X. L. Ping, Y. S. Chen, W. J. Wang, K. X. Jin, X. Wang, C. M. Huang, Y. Fu, X. M. Ge, S. H. Song, H. S. Jeong, H. Yanagisawa, Y. Niu, G. F. Jia, W. Wu, W. M. Tong, A. Okamoto, C. He, J. M. Rendtlew Danielsen, X. J. Wang, Y. G. Yang, FTO-dependent demethylation of N6-methyladenosine regulates mRNA splicing and is required for adipogenesis. *Cell Res.* **24**, 1403–1419 (2014).
26. B. Chen, F. Ye, L. Yu, G. Jia, X. Huang, X. Zhang, S. Peng, K. Chen, M. Wang, S. Gong, R. Zhang, J. Yin, H. Li, Y. Yang, H. Liu, J. Zhang, H. Zhang, A. Zhang, H. Jiang, C. Luo, C. G. Yang, Development of cell-active N^6-methyladenosine RNA demethylase FTO inhibitor. *J. Am. Chem. Soc.* **134**, 17963–17971 (2012).
27. Y. Huang, J. Yan, Q. Li, J. Li, S. Gong, H. Zhou, J. Gan, H. Jiang, G. F. Jia, C. Luo, C. G. Yang, Meclofenamic acid selectively inhibits FTO demethylation of m^6A over ALKBH5. *Nucleic Acids Res.* **43**, 373–384 (2015).
28. W. Aik, M. Demetriades, M. K. Hamdan, E. A. Bagg, K. K. Yeoh, C. Lejeune, Z. Zhang, M. A. McDonough, C. J. Schofield, Structural basis for inhibition of the fat mass and obesity associated protein (FTO). *J. Med. Chem.* **56**, 3680–3688 (2013).
29. J. D. W. Toh, L. Sun, L. Z. M. Lau, J. Tan, J. J. A. Low, C. W. Q. Tang, E. J. Y. Cheong, M. J. H. Tan, Y. Chen, W. Hong, Y. G. Gao, E. C. Y. Woon, A strategy based on nucleotide specificity leads to a subfamily-selective and cell-active inhibitor of N^6-methyladenosine demethylase FTO. *Chem. Sci.* **6**, 112–122 (2015).
30. W. He, B. Zhou, W. Liu, M. Zhang, Z. Shen, Z. Han, Q. Jiang, Q. Yang, C. Song, R. Wang, T. Niu, S. Han, L. Zhang, J. Wu, F. Guo, R. Zhao, W. Yu, J. Chai, J. Chang, Identification of a novel small-molecule binding site of the fat mass and obesity associated protein (FTO). *J. Med. Chem.* **58**, 7341–7348 (2015).
31. G. Zheng, T. Cox, L. Tribbey, G. Z. Wang, P. Iacoban, M. E. Booher, G. J. Gabriel, L. Zhou, N. Bae, J. Rowles, C. He, M. J. Olsen, Synthesis of a FTO inhibitor with anticonvulsant activity. *ACS Chem. Nerosci.* **5**, 658–665 (2014).
32. E. Nissinen, I. B. Lindén, E. Schultz, P. Pohto, Biochemical and pharmacological properties of a peripherally acting catechol-O-methyltransferase inhibitor entacapone. *Naunyn Schmiedebergs Arch. Pharmacol.* **346**, 262–266 (1992).
33. R. Cao, M. Liu, M. Yin, Q. Liu, Y. Wang, N. Huang, Discovery of novel tubulin inhibitors via structure-based hierarchical virtual screening. *J. Chem. Inf. Model.* **52**, 2730–2740 (2012).
34. N. Huang, C. Kalyanaraman, J. J. Irwin, M. P. Jacobson, Physics-based scoring of protein-ligand complexes: Enrichment of known inhibitors in large-scale virtual screening. *J. Chem. Inf. Model.* **46**, 243–253 (2006).
35. X. Lin, X. P. Huang, G. Chen, R. Whaley, S. Peng, Y. Wang, G. Zhang, S. X. Wang, S. Wang, B. L. Roth, N. Huang, Life beyond kinases: Structure-based discovery of sorafenib as nanomolar antagonist of 5-HT receptors. *J. Med. Chem.* **55**, 5749–5759 (2012).
36. N. Huang, B. K. Shoichet, J. J. Irwin, Benchmarking sets for molecular docking. *J. Med. Chem.* **49**, 6789–6801 (2006).
37. B. K. Shoichet, Virtual screening of chemical libraries. *Nature* **432**, 862–865 (2004).
38. M. Vinogradova, V. S. Gehling, A. Gustafson, S. Arora, C. A. Tindell, C. Wilson, K. E. Williamson, G. D. Guler, P. Gangurde, W. Manieri, J. Busby, E. M. Flynn, F. Lan, H. J. Kim, S. Odate, A. G. Cochran, Y. Liu, M. Wongchenko, Y. Yang, T. K. Cheung, T. M. Maile, T. Lau, M. Costa, G. V. Hegde, E. Jackson, R. Pitti, D. Arnott, C. Bailey, S. Bellon, R. T. Cummings, B. K. Albrecht, J. C. Harmange, J. R. Kiefer, P. Trojer, M. Classon, An inhibitor of KDM5 demethylases reduces survival of drug-tolerant cancer cells. *Nat. Chem. Biol.* **12**, 531–538 (2016).
39. A. Eijkelenboom, B. M. Burgering, FOXOs: Signalling integrators for homeostasis maintenance. *Nat. Rev. Mol. Cell Biol.* **14**, 83–97 (2013).
40. Y. Liu, R. Dentin, D. Chen, S. Hedrick, K. Ravnskjaer, S. Schenk, J. Milne, D. J. Meyers, P. Cole, J. Yates III, J. Olefsky, L. Guarente, M. Montminy, A fasting inducible switch modulates gluconeogenesis via activator/coactivator exchange. *Nature* **456**, 269–273 (2008).
41. T. Nagashima, N. Shigematsu, R. Maruki, Y. Urano, H. Tanaka, A. Shimaya, T. Shimokawa, M. Shibasaki, Discovery of novel forkhead box O1 inhibitors for treating type 2 diabetes: Improvement of fasting glycemia in diabetic db/db mice. *Mol. Pharmacol.* **78**, 961–970 (2010).
42. D. N. Gross, A. P. van den Heuvel, M. J. Birnbaum, The role of FoxO in the regulation of metabolism. *Oncogene* **27**, 2320–2336 (2008).
43. F. Langlet, R. A. Haeusler, D. Lindén, E. Ericson, T. Norris, A. Johansson, J. R. Cook, K. Aizawa, L. Wang, C. Buettner, D. Accili, Selective inhibition of FOXO1 activator/repressor balance modulates hepatic glucose handling. *Cell* **171**, 824–835.e18 (2017).
44. E. E. Zhang, Y. Liu, R. Dentin, P. Y. Pongsawakul, A. C. Liu, T. Hirota, D. A. Nusinow, X. Sun, S. Landais, Y. Kodama, D. A. Brenner, M. Montminy, S. A. Kay, Cryptochrome mediates circadian regulation of cAMP signaling and hepatic gluconeogenesis. *Nat. Med.* **16**, 1152–1156 (2010).
45. A. Bartelt, J. Heeren, Adipose tissue browning and metabolic health. *Nat. Rev. Endocrinol.* **10**, 24–36 (2014).

46. M. Harms, P. Seale, Brown and beige fat: Development, function and therapeutic potential. *Nat. Med.* **19**, 1252–1263 (2013).
47. T. Inagaki, J. Sakai, S. Kajimura, Transcriptional and epigenetic control of brown and beige adipose cell fate and function. *Nat. Rev. Mol. Cell Biol.* **17**, 480–495 (2016).
48. J. Wu, P. Cohen, B. M. Spiegelman, Adaptive thermogenesis in adipocytes: Is beige the new brown? *Genes Dev.* **27**, 234–250 (2013).
49. A. Ortega-Molina, A. Efeyan, E. Lopez-Guadamillas, M. Muñoz-Martin, G. Gómez-López, M. Cañamero, F. Mulero, J. Pastor, S. Martinez, E. Romanos, M. Mar Gonzalez-Barroso, E. Rial, A. M. Valverde, J. R. Bischoff, M. Serrano, Pten positively regulates brown adipose function, energy expenditure, and longevity. *Cell Metab.* **15**, 382–394 (2012).
50. J. Nakae, Y. Cao, M. Oki, Y. Orba, H. Sawa, H. Kiyonari, K. Iskandar, K. Suga, M. Lombes, Y. Hayashi, Forkhead transcription factor FoxO1 in adipose tissue regulates energy storage and expenditure. *Diabetes* **57**, 563–576 (2008).
51. D. Babovic, C. M. O'Tuathaigh, A. M. O'Connor, G. J. O'Sullivan, O. Tighe, D. T. Croke, M. Karayiorgou, J. A. Gogos, D. Cotter, J. L. Waddington, Phenotypic characterization of cognition and social behavior in mice with heterozygous versus homozygous deletion of catechol-*O*-methyltransferase. *Neuroscience* **155**, 1021–1029 (2008).
52. D. Babovic, C. M. O'Tuathaigh, G. J. O'Sullivan, J. J. Clifford, O. Tighe, D. T. Croke, M. Karayiorgou, J. A. Gogos, D. Cotter, J. L. Waddington, Exploratory and habituation phenotype of heterozygous and homozygous COMT knockout mice. *Behav. Brain Res.* **183**, 236–239 (2007).
53. K. Annerbrink, L. Westberg, S. Nilsson, R. Rosmond, G. Holm, E. Eriksson, Catechol O-methyltransferase val158-met polymorphism is associated with abdominal obesity and blood pressure in men. *Metabolism* **57**, 708–711 (2008).
54. M. Kanasaki, S. P. Srivastava, F. Yang, L. Xu, S. Kudoh, M. Kitada, N. Ueki, H. Kim, J. Li, S. Takeda, K. Kanasaki, D. Koya, Deficiency in catechol-o-methyltransferase is linked to a disruption of glucose homeostasis in mice. *Sci. Rep.* **7**, 7927 (2017).
55. D. E. Chusyd, D. Wang, D. M. Huffman, T. R. Nagy, Relationships between rodent white adipose fat pads and human white adipose fat depots. *Front. Nutr.* **3**, 10 (2016).
56. X. Liu, C. Cervantes, F. Liu, Common and distinct regulation of human and mouse brown and beige adipose tissues: A promising therapeutic target for obesity. *Protein Cell* **8**, 446–454 (2017).
57. J. J. Irwin, F. M. Raushel, B. K. Shoichet, Virtual screening against metalloenzymes for inhibitors and substrates. *Biochemistry* **44**, 12316–12328 (2005).
58. J. J. Irwin, T. Sterling, M. M. Mysinger, E. S. Bolstad, R. G. Coleman, ZINC: A free tool to discover chemistry for biology. *J. Chem. Inf. Model.* **52**, 1757–1768 (2012).
59. D. M. Lorber, B. K. Shoichet, Hierarchical docking of databases of multiple ligand conformations. *Curr. Top. Med. Chem.* **5**, 739–749 (2005).
60. M. M. Mysinger, B. K. Shoichet, Rapid context-dependent ligand desolvation in molecular docking. *J. Chem. Inf. Model.* **50**, 1561–1573 (2010).
61. B. Q. Wei, W. A. Baase, L. H. Weaver, B. W. Matthews, B. K. Shoichet, A model binding site for testing scoring functions in molecular docking. *J. Mol. Biol.* **322**, 339–355 (2002).
62. Z. Otwinowski, W. Minor, Processing of x-ray diffraction data collected in oscillation mode. *Methods Enzymol.* **276**, 307–326 (1997).
63. P. Emsley, B. Lohkamp, W. G. Scott, K. Cowtan, Features and development of coot. *Acta Crystallogr. D Biol. Crystallogr.* **66**, 486–501 (2010).
64. G. N. Murshudov, P. Skubák, A. A. Lebedev, N. S. Pannu, R. A. Steiner, R. A. Nicholls, M. D. Winn, F. Long, A. A. Vagin, REFMAC5 for the refinement of macromolecular crystal structures. *Acta Crystallogr. D Biol. Crystallogr.* **67**, 355–367 (2011).
65. G. Tiscornia, O. Singer, I. M. Verma, Production and purification of lentiviral vectors. *Nat. Protoc.* **1**, 241–245 (2006).
66. R. Wu, X. M. Liu, J. G. Sun, H. Chen, J. Ma, M. Dong, S. Peng, J. Q. Wang, J. Q. Ding, D. H. Li, J. R. Speakman, G. Ning, W. Jin, Z. Yuan, DJ-1 maintains energy and glucose homeostasis by regulating the function of brown adipose tissue. *Cell Discovery* **3**, 16054 (2017).
67. P. Liu, N. A. Jenkins, N. G. Copeland, A highly efficient recombineering-based method for generating conditional knockout mutations. *Genome Res.* **13**, 476–484 (2003).
68. Y. Naito, K. Hino, H. Bono, K. Ui-Tei, CRISPRdirect: Software for designing CRISPR/Cas guide RNA with reduced off-target sites. *Bioinformatics* **31**, 1120–1123 (2015).
69. C. Zhang, Y. Chen, B. Sun, L. Wang, Y. Yang, D. Ma, J. Lv, J. Heng, Y. Ding, Y. Xue, X. Lu, W. Xiao, Y. G. Yang, F. Liu, m^{6}A modulates haematopoietic stem and progenitor cell specification. *Nature* **549**, 273–276 (2017).
70. T. Chen, Y. J. Hao, Y. Zhang, M. M. Li, M. Wang, W. Han, Y. Wu, Y. Lv, J. Hao, L. Wang, A. Li, Y. Yang, K. X. Jin, X. Zhao, Y. Li, X. L. Ping, W. Y. Lai, L. G. Wu, G. Jiang, H. L. Wang, L. Sang, X. J. Wang, Y. G. Yang, Q. Zhou, m^{6}A RNA methylation is regulated by microRNAs and promotes reprogramming to pluripotency. *Cell Stem Cell* **16**, 289–301 (2015).
71. A. M. Bolger, M. Lohse, B. Usadel, Trimmomatic: A flexible trimmer for Illumina sequence data. *Bioinformatics* **30**, 2114–2120 (2014).
72. C. Trapnell, L. Pachter, S. L. Salzberg, TopHat: Discovering splice junctions with RNA-seq. *Bioinformatics* **25**, 1105–1111 (2009).
73. S. Anders, P. T. Pyl, W. Huber, HTSeq—A python framework to work with high-throughput sequencing data. *Bioinformatics* **31**, 166–169 (2015).
74. L. Wang, Z. Feng, X. Wang, X. Wang, X. Zhang, DEGseq: An R package for identifying differentially expressed genes from RNA-seq data. *Bioinformatics* **26**, 136–138 (2010).
75. W. Huang da, B. T. Sherman, R. A. Lempicki, Bioinformatics enrichment tools: Paths toward the comprehensive functional analysis of large gene lists. *Nucleic Acids Res.* **37**, 1–13 (2009).
76. Y. Zhang, T. Liu, C. A. Meyer, J. Eeckhoute, D. S. Johnson, B. E. Bernstein, C. Nusbaum, R. M. Myers, M. Brown, W. Li, X. S. Liu, Model-based analysis of ChIP-seq (MACS). *Genome Biol.* **9**, R137 (2008).
77. S. Heinz, C. Benner, N. Spann, E. Bertolino, Y. C. Lin, P. Laslo, J. X. Cheng, C. Murre, H. Singh, C. K. Glass, Simple combinations of lineage-determining transcription factors prime cis-regulatory elements required for macrophage and B cell identities. *Mol. Cell* **38**, 576–589 (2010).
78. A. R. Quinlan, I. M. Hall, BEDTools: A flexible suite of utilities for comparing genomic features. *Bioinformatics* **26**, 841–842 (2010).

Acknowledgments: We thank the staff at the Shanghai Synchrotron Radiation Facility (SSRF) for assistance in data collection. We thank M. Montminy (The Salk Institute for Biological Studies) for providing the *G6PC*:Luc plasmid, B. Zhu [Institute of Biophysics, Chinese Academy of Sciences (CAS)] for TET1 protein, and Z. Yuan for pGL4.23-Ucp1-luciferase and pGL4.23 control constructs and pRenilla-TK plasmid (Institute of Biophysics, CAS). **Funding:** This work was supported by Strategic Priority Research Program A of the CAS (XDA16000000 to Y.-G.Y.), the National Natural Science Foundation of China (NSFC) (31625016 to Y.-G.Y.), the National Basic Research Program of China (2014CB849802 to N. Huang and 2016YFC0900300 to Y.-G.Y.), the National Major Scientific and Technological Special Project for "Significant New Drugs Development" (2013ZX09509102 to N. Huang), the CAS Strategic Priority Research Program (XDB14030300/QYZDY-SSW-SMC027 to Y.-G.Y.), Youth Innovation Promotion Association (CAS 2016097 to B.S.), and the Chinese "Recruitment Program of Global Youth Experts" (to E.E.Z.). Computational support was provided by the Special Program for Applied Research on Super Computation of the NSFC–Guangdong Joint Fund (the second phase) under grant no. U1501501 (to N. Huang). **Author contributions:** N. Huang, E.E.Z., and Y.-G.Y. designed experiments. S.P. and N. Huang performed the computational screening and designed the structure-activity relationship studies. Yanli Wang and W.Z. purified proteins. S.P. performed the enzymatic activity assays and SPR binding assays. Yanli Wang, R.C., and W.Z. performed the crystallization and structural determination. D.J., W.X., and Q.L. performed cellular functional studies. H.Z, D.J., S.Z., P.L., N. Hou, Y.N., S.P., and G.Z. performed animal studies. N. Hou, G.Z., L.Z., and F.W. generated the FTO conditional knockout mice and FOXO1 mutant mice. B.S., W.X., C.G., and Q.L. performed RNA-seq and m^{6}A-seq studies of adipose tissues and analyzed data. H.H. and T.C. performed RNA-seq studies and data analysis in Hep-G2 cells. Yankai Wang and S.H. synthesized DNA and RNA oligos. W.L., H.W., Y.M., and Z.Z. performed liquid chromatography–tandem mass spectrometry experiments. Z.M. contributed reagents and cell lines. S.P., D.J., W.X., B.S., Y.-L.Z., Y.-G.Y., E.E.Z., and N. Huang analyzed the data and wrote the manuscript. All authors discussed the results and commented on the manuscript. **Competing interests:** G.Z. and N. Huang have equity interest in RPXDs (Suzhou) Co. Ltd., which develops FTO inhibitors for the treatment of metabolic disorders. N. Huang, G.Z., S.P., and N. Hou hold an international patent (United States, 14147531; European, 13858101.2; Chinese, 201210497436.7 and 201380071479.1; Australia, 2013351676; Canada, 2892902) on the use of entacapone for prevention and treatment of obesity and related metabolic diseases. **Data and materials availability:** The coordinates and structure factors for the crystal complex structure of FTO-entacapone and FTO–cpd-7 were deposited in the PDB with PDB codes 6AK4 and 6AEJ, respectively. The m^{6}A-seq and RNA-seq data have been deposited in the Gene Expression Omnibus (GEO) database under accession numbers GSE106998, GSE107411, GSE125785, and GSE125786 and have also been deposited in the GSA database (http://gsa.big.ac.cn/) under accession number PRJCA000645. All data associated with this study are present in the paper or the Supplementary Materials.

Submitted 4 October 2018
Accepted 25 March 2019
Published 17 April 2019
10.1126/scitranslmed.aau7116

Citation: S. Peng, W. Xiao, D. Ju, B. Sun, N. Hou, Q. Liu, Y. Wang, H. Zhao, C. Gao, S. Zhang, R. Cao, P. Li, H. Huang, Y. Ma, Y. Wang, W. Lai, Z. Ma, W. Zhang, S. Huang, H. Wang, Z. Zhang, L. Zhao, T. Cai, Y.-L. Zhao, F. Wang, Y. Nie, G. Zhi, Y.-G. Yang, E. E. Zhang, N. Huang, Identification of entacapone as a chemical inhibitor of FTO mediating metabolic regulation through FOXO1. *Sci. Transl. Med.* **11**, eaau7116 (2019).

Science Translational Medicine

Identification of entacapone as a chemical inhibitor of FTO mediating metabolic regulation through FOXO1

Shiming Peng, Wen Xiao, Dapeng Ju, Baofa Sun, Nannan Hou, Qianlan Liu, Yanli Wang, Haijiao Zhao, Chunchun Gao, Song Zhang, Ran Cao, Pengfei Li, Huanwei Huang, Yongfen Ma, Yankai Wang, Weiyi Lai, Zhixiong Ma, Wei Zhang, Song Huang, Hailin Wang, Zhiyuan Zhang, Liping Zhao, Tao Cai, Yong-Liang Zhao, Fengchao Wang, Yongzhan Nie, Gang Zhi, Yun-Gui Yang, Eric Erquan Zhang and Niu Huang

Sci Transl Med **11**, eaau7116.
DOI: 10.1126/scitranslmed.aau7116

The skinny on FTO

Although the fat mass and obesity-associated gene *FTO* has been linked to genetic risk of obesity, the mRNA demethylase that it encodes has proven difficult to therapeutically target. From a screen of approved drugs, Peng *et al*. identified entacapone, a catechol-*O*-methyltransferase inhibitor used in the treatment of Parkinson's disease, as an inhibitor of FTO. In vivo administration of entacapone improved body weight and glucose tolerance and increased adipose thermogenesis in mice, which the authors tied to decreased FTO-catalyzed m^6A demethylation of *FOXO1* mRNA. Further studies will need to confirm the repurposing potential of entacapone for obesity or metabolic disease in humans.